Appl Phys A (2009) 94: 949–955
DOI 10.1007/s00339-008-4873-8

Applied Physics A
Materials Science & Processing

Nanosecond pulsed laser ablation of silicon in liquids

R. Karimzadeh · J. Zamir Anvari · N. Mansour

Received: 18 February 2008 / Accepted: 6 August 2008 / Published online: 9 September 2008
© Springer-Verlag 2008

Abstract Laser fluence and laser shot number are important parameters for pulse laser based micromachining of silicon in liquids. This paper presents laser-induced ablation of silicon in liquids of the dimethyl sulfoxide (DMSO) and the water at different applied laser fluence levels and laser shot numbers. The experimental results are conducted using 15 ns pulsed laser irradiation at 532 nm. The silicon surface morphology of the irradiated spots has an appearance as one can see in porous formation. The surface morphology exhibits a large number of cavities which indicates as bubble nucleation sites. The observed surface morphology shows that the explosive melt expulsion could be a dominant process for the laser ablation of silicon in liquids using nanosecond pulsed laser irradiation at 532 nm. Silicon surface's ablated diameter growth was measured at different applied laser fluences and shot numbers in both liquid interfaces. A theoretical analysis suggested investigating silicon surface etching in liquid by intense multiple nanosecond laser pulses. It has been assumed that the nanosecond pulsed laser-induced silicon surface modification is due to the process of explosive melt expulsion under the action of the confined plasma-induced pressure or shock wave trapped between the silicon target and the overlying liquid. This analysis allows us to determine the effective lateral interaction zone of ablated solid target related to nanosecond pulsed laser illumination. The theoretical analysis is found in excellent agreement with the experimental measurements of silicon ablated diameter growth in the DMSO and the water interfaces. Multiple-shot laser ablation threshold of silicon is determined. Pulsed energy accumulation model is used to obtain the single-shot ablation threshold of silicon. The smaller ablation threshold value is found in the DMSO, and the incubation effect is also found to be absent.

PACS 52.38.Mf · 61.82.Fk · 81.65.Cf · 52.38.-r · 62.50.Ef

1 Introduction

There is a great deal of interest in nanosecond pulsed lasers ablation of solid materials because of its great potential in laser-based material processing including thin solid film preparation, synthesis of nanostructures, material surface cleaning, and microelectronic device fabrication. An important requirement in the laser-assisted micromachining of solids is the production of high-quality machined surfaces. In the case of laser ablation, the surface of the ablated material is usually surrounded by redeposition of etched material or debris that has to be subsequently removed by other methods. An alternative would be to remove it during the laser ablation process itself. This can be accomplished by laser material processing under liquid confinement. There are other advantages of liquid-assisted laser material processing including development of higher plasma pressure due to confinement, more effective cooling, reduced noise level, and higher optical breakdown threshold than that of air [1–3].

Laser processing of silicon has been an area of intense fundamental and applied research for many years. Several studies have been reported on pulsed laser ablation of silicon in vacuum [4], air [5], and gasses [6]. Liquid-assisted processes have been introduced as an efficient technique for silicon laser-based microprocessing [7–9]. For example, Ren et al. [10] have investigated laser ablation of silicon underwater over a broad range of applied laser irradiances

R. Karimzadeh · J.Z. Anvari · N. Mansour (✉)
Department of Physics, Shahid Beheshti University, Evin, Tehran 19839, Iran
e-mail: n-mansour@cc.sbu.ac.ir
Fax: +98-21-22431666

(5 to 80 GW/cm^2) using a third harmonic of Nd:YAG laser with pulse a duration of 5 ns at a wavelength of 355 nm. A twofold increase in the ablation rate was achieved in the water compared to the results measured in the air. They reported that the water layer effectively reduces the oxidation and redeposition of the ablation-removed particles, most likely owing to the reduced oxygen contact, the effect of amplified pressure, and bubble formation with the subsequent convective motion of the liquid jet and additional shock pressure.

Zhu et al. [3] have investigated laser ablation of silicon using a KrF excimer laser with a wavelength of 248 nm and pulse duration of 23 ns. They have reported that laser ablation rate is highly enhanced by the presence of the water interface compared with the ablation rate results found in the air. In their analysis, it has been assumed that the plasma generated in the water confinement region induces a much higher pressure. Once generated, the plasma expands adiabatically at a supersonic velocity, creating a shock wave in front. The high-pressure and high-temperature plasma causes evaporation of silicon target with higher ablation rate. Choo et al. [11] have studied the silicon laser ablation by 25 ns KrF laser beam at 248 nm in air and underwater. The silicon ablated regions were characterized using conventional optical and scanning electron microscope as well as a laser interference microscope. Their results showed significant differences in the nature of laser ablation in air and underwater. For example, while the ablated surface is smooth in the case of machining in air, it is somewhat rough in the case of machining underwater. They have reported that the induced surface modification in the case of laser processing underwater shows the results of molten silicon rapidly solidified with a dendrite structure. Their results have indicated the absence of ablation process due to the thermal evaporation of silicon in the case of machining underwater.

Yoo et al. [12] have studied the mass removed from a single-crystal silicon samples by high irradiance (1 to 100 GW/cm^2) using Nd:YAG laser which emits 3 ns pulses at 266 nm by quadrupling the fundamental frequency. The single-pulse laser ablation was studied by measuring the resulting crater morphology with a white light interferometer microscope. They demonstrated that the thermal evaporation alone is an inadequate process to account for the measured ablated depth data. The evaporating vapor can exert a recoil pressure on the melted surface, and molten mass can be pushed outward from the irradiated zone. The formation of a deep superheated liquid layer with subsequent explosive boiling has been introduced as the responsible mechanisms for melt ejection.

Andreic et al. [13] have reported the results of laser ablation of single-crystal silicon with nitrogen laser radiation at wavelength of 337 nm, pulse length of 6 ns, at energy density of 1.1 J/cm^2. Many micrometer droplets were observed around the ablated target area. The droplets were most probably produced within a single laser pulse as a result of hydrodynamic instability of the molten surface layer. They pointed out that the intense splashing of silicon droplets occurs as a consequence of the large plasma pressure generated by the most intense parts of the laser beam.

The neutral liquid DMSO has also been reported as a useful interface for obtaining high etch rate in poly-SiC [2, 14, 15]. Shafeev et al. [16–18] measured the ablation rate of a diamond in the DMSO as high as 50 μm/s using 10 ns pulsed copper-vapor laser irradiation.

The aim of the present study is to investigate laser fluence and shot number dependences of the nanosecond pulse laser ablation of silicon in underwater and the DMSO confinements. The silicon ablation is studied using the second harmonic of Nd:YAG laser emitting a beam at 532 nm with pulse duration of 15 ns. We analyze the experimental observations of laser-induced surface modification of silicon under repetitive irradiation at different applied laser fluence levels. For determining the ablation threshold, the ablated diameters on the silicon surface is measured at various applied laser fluences and shot numbers using nanosecond pulsed laser irradiation with fluence range of 4 to 11 J/cm^2. A theoretical analysis has suggested to investigate the silicon ablation in liquid by intense multiple nanosecond laser pulses. It is assumed that the nanosecond pulsed laser-induced surface ablation of silicon is due to the process of melt expulsion under the action of the confined plasma-induced pressure or shock wave trapped between the silicon target and the overlying liquid. We will show that the presented theoretical analysis allows us to determine the multiple-shot ablation threshold of silicon in the DMSO and the water interfaces using the experimental measurements of the surface ablation diameter growth. Pulsed energy accumulation model is used to obtain the single-shot ablation threshold of silicon in the DMSO and the water.

The details of used experimental setup and samples are given in Sect. 2. In Sect. 3, the experimental results of laser-induced surface modification of silicon under a repetitive irradiation at different applied laser fluence levels are presented. A theoretical analysis for determining the nanosecond pulsed laser ablation threshold is investigated. The conclusions are given in Sect. 4.

2 Experimental details

The n-type (100) silicon wafer have been irradiated in the DMSO and the water with a normally incident second harmonic of Nd:YAG laser beam. The laser generated 15 ns pulses at 532 nm. The silicon samples were irradiated with the laser fluence range of 4–11 J/cm^2, and the laser repetition rate was 1 Hz. The silicon wafers were mounted on

a three-axis translation stage. The sample was set vertically inside a glass container provided with an optical window for a laser irradiation. The laser pulses were focused with a 50 cm focal length lens. The spatial profile of the laser pulse was Gaussian, with a 150 µm beam waist $(HW1/e^2M)$ at the target. The surface morphology of pulsed laser irradiated samples was obtained by scanning electron microscopy (SEM). The diameter of silicon ablated regions were determined by Nomarski optical microscope.

3 Experimental results and discussion

Under an exposure of silicon sample to five laser pulses in the DMSO at applied laser fluence level of about 5 J/cm^2, a significant change in the surface morphology was observed (Fig. 1a). We must mention that the surface features start to form only when plasma appears in the front of the silicon surface. The laser-induced surface structures are not ordered with no uniform structures spacing. The silicon surface morphology of the irradiated spots has an appearance as one can see in the porous formation (Fig. 1a). The surface morphology exhibits a formation of a large number of cavities which indicates as bubble nucleation sites. The number of bubble nucleation site increases by increasing the applied laser fluence. Some of the details of the silicon ablated region are shown at higher magnifications in Fig. 1b. It is worth noting the presence of round-shaped cavities. It seems that such round-shaped cavities are the sites of bubble nucleation initiated by the boiling which afterwards escape from the molten liquid. As one can see in Fig. 1b, some of the bubbles escaped while the others were trapped and did not escape the liquid before it resolidified.

Figure 2a shows the morphology of the silicon surface irradiated in the water with five pulses at applied laser fluence level of 7 J/cm^2. The silicon surface morphology of the irradiated spots in the water includes very similar surface features to the ablated spots in the DMSO. However, a limited number of bubble nucleation sites are formed during the laser ablation of silicon in the water (see Fig. 2b).

The silicon nanosecond pulsed laser ablation mechanisms in liquid interface require the identification of the dominant energy transport processes. Nanosecond pulsed laser illumination of silicon in liquid interface with high irradiance of 1 to 10 GW/cm^2 creates confined high-pressure and high-temperature plasma [11, 19, 20]. This leads to the generation of high density of excited electrons within the target interaction zone which can easily transfer energy to phonons during electron–phonon relaxation [21]. The energy is redistributed through a lattice vibration and consequently the heat is conducted in the silicon target. This heat may melt or vaporize the sample. It is worth noting that the observed silicon surface morphology of the irradiated spots

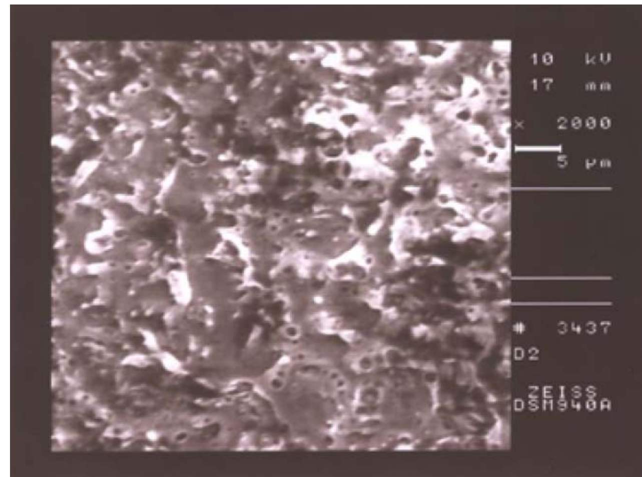

Fig. 1a Shows SEM image of the irradiated silicon surface morphology under the DMSO by five 532 nm laser pulses at a fluence of 5 J/cm^2

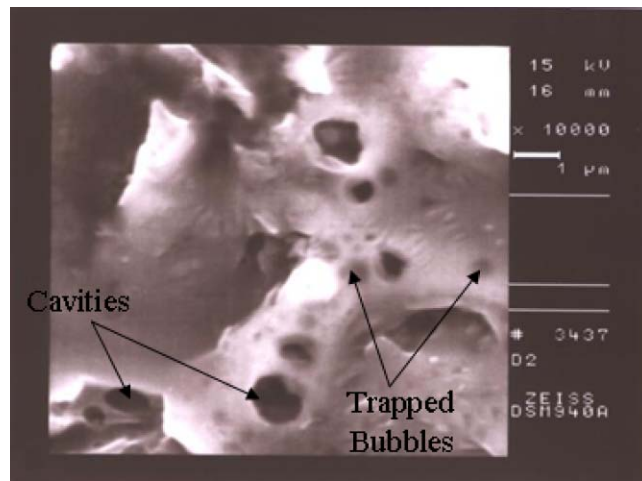

Fig. 1b High-magnification SEM image of irradiated surface morphology of silicon under the DMSO confinement by five 532 nm laser pulses at a fluence of 5 J/cm^2 indicates cavities several as bubble nucleation sites and some as trapped bubbles

includes a large number of cavities and trapped bubble sites. This indicates that an explosive melt expulsion could be a dominant process for the laser ablation of silicon in liquids using nanosecond pulsed laser irradiation at 532 nm.

A frequently used technique for determining the ablation threshold of solid targets using the ultrashort pulse lasers (femtosecond and picosecond pulsed laser) with Gaussian spatial profile is to measure the diameter of the ablated regions induced on the target surface at various applied laser fluences and shot numbers [22–26]. Compared with nanosecond pulsed lasers, ultrashort pulses significantly alter the processes associated with an ablation. Rapid energy deposition reduces both the liquid phase and the heat-affected zone which are both usually present during the laser

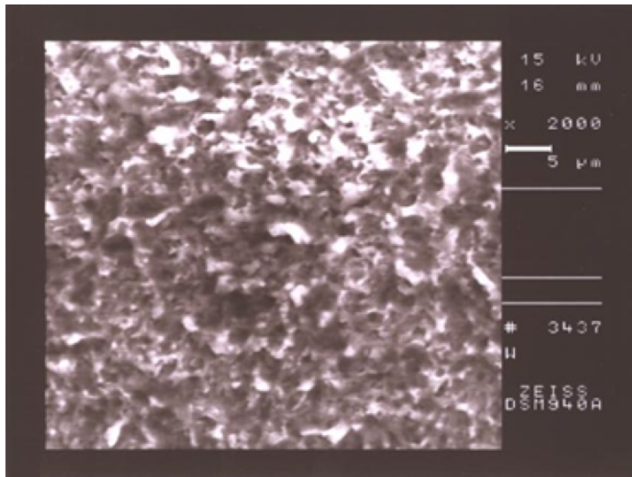

Fig. 2a Shows SEM image of the irradiated silicon surface morphology underwater by five 532 nm laser pulses at a fluence of 7 J/cm^2

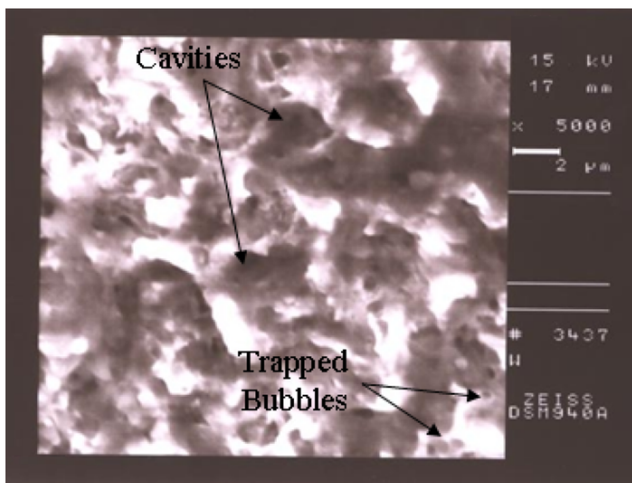

Fig. 2b High-magnification SEM image of irradiated surface morphology of silicon underwater by five 532 nm laser pulses at a fluence of 7 J/cm^2 indicates cavities several as bubble nucleation sites and some as trapped bubbles

ablation [27]. In these cases, lateral dimensions of the laser generated craters are used to measure the ablation threshold in many solid materials using a femtosecond and a picosecond pulsed laser irradiations [28]. For a Gaussian beam illumination, the spatial fluence profile $F(r)$ is given by:

$$F(r) = F_0 \exp\left(-\frac{2r^2}{\omega_0^2}\right) \tag{1}$$

where r represents the distance from the beam center, ω_0 is the $1/e^2$-radius of the distribution, and F_0 denotes the maximum laser fluence at the cross-sectional surface. The maximum fluence and the pulse energy E_p are directly related by:

$$F_0 = \frac{2E_p}{\pi\omega_0^2}. \tag{2}$$

With an ablation threshold fluence, F_{th}, the diameter, D, of an ablated crater is also related to the maximum fluence [25]:

$$D^2 = 2\omega_0^2\big[\ln(F_0) - \ln(F_{\text{th}})\big]. \tag{3}$$

Due to the linear dependence of the maximum laser fluence on the total pulse energy (3), it is possible to determine both the beam radius and hence the threshold fluence from the plot of the square of the crater diameter versus the logarithm of the applied laser fluence. This technique is used to evaluate the ablation threshold of various materials using a femtosecond and a picosecond pulsed laser irradiations [22–26, 28].

To illustrate the laser fluence and shot number dependence of nanosecond pulsed laser induced ablation of silicon in the DMSO and the water, several etched spots in arrays were generated on a surface of the sample. Our results show that the square of ablated spots diameter increases linearly with the logarithm of the applied laser fluence. Using (3), the estimated laser beam spot sizes in the DMSO and the water were obtained as 290 ± 10 μm and 326 ± 8 μm, respectively. However, the laser beam spot size was measured to be 150 μm. This means that (3) is not able to predict the correct value of the laser spot size. The rapid energy deposition or ultrashort pulsed laser-induced confined interaction zone of material is not a valid assumption in the case of nanosecond laser pulses. Further investigation is required to evaluate the effective lateral interaction zone of ablated solid target related to a nanosecond pulsed laser illumination. In the paragraphs to follow, we will present a theoretical analysis investigating the silicon surface etching in liquid by intense multiple nanosecond laser pulses.

When irradiating a solid target confined in a liquid with a high-intensity focused nanosecond pulsed laser beam, the laser energy is absorbed in a thin layer and high-pressure plasma is generated. The laser-induced plasma adiabatically expands at a supersonic velocity to create a shock wave under the confinement of a liquid. The shock wave or plasma-induced pressure trapped between the target and the overlying liquid. Further, more energy deposition by the remaining of a laser pulse will lead to a temperature increase of a laser-induced plasma and induce higher amplitudes for shock waves [29–33]. The nanosecond pulsed laser-induced plasma obtained in the water-confined regime induces peak pressure as high as 5.5 GPa [33]. Therefore, the shock wave generated by the laser-induced plasma pushes the confined plasma into a thermodynamic state of the higher temperature, higher pressure, and higher density of the plasma.

These processes provide a continual energy source during the pulse width of the confined plasma for ablation of materials. It has been reported [32] that the liquid-confined plasma pulse width is 2–3 times longer than the applied laser pulse duration.

We treat the plasma as an ideal gas confined between two pistons with the piston separation L and the laser-induced plasma pressure or shock wave P. The temporal behaviors of L and P are given by [29, 30]:

$$\frac{dP}{dt} = \frac{fI(r,t) - (1+\frac{3}{2\alpha})\frac{2P^2}{Z}}{\frac{3}{2\alpha}L}, \tag{4}$$

$$\frac{dL}{dt} = \frac{2}{Z}P, \tag{5}$$

where f is the fraction of driver laser energy absorbed by an ideal gas, and α is the fraction of the internal energy devoted to the thermal energy (typically, $\alpha = 0.4$). Z is the reduced shock impedance between the target (Z_t) and the confining liquid (Z_l) given by [3]:

$$\frac{2}{Z} = \frac{1}{Z_t} + \frac{1}{Z_l}. \tag{6}$$

In (4), we assume that the ideal gas is heated by a laser pulse with a temporal profile of $T(t)$ and the Gaussian spatial profile form given by:

$$I(r,t) = I_0 T(t) e^{-\frac{2r^2}{\omega_0^2}}, \tag{7}$$

where ω_0 is the $1/e^2$-radius of the distribution and I_0 denotes the laser peak irradiance. Under assumption that the $T(t)$ can remain constant during the laser pulse width [29, 30], the plasma pressure is obtained using (4) and (5) as:

$$P = \left(\frac{1}{2}\frac{fZ}{(1+\frac{3}{2\alpha})\tau}F_0\right)^{1/2} e^{-\frac{r^2}{\omega_0^2}}. \tag{8}$$

With $I_0 = \frac{F_0}{\tau}$ and τ is the laser pulse width. Note that the spot size of the shock wave profile increased by a factor of $\sqrt{2}$ compared to the applied laser beam spot size.

The laser beam that reaches the sample surface through the plasma plume is absorbed into the sample and it melts the layer. The irradiated surface can be thought of a piston that exerts pressure equal to P (8) on the melt. The piston will squirt the melt out of the crater at wilt velocity (v_{ej}) given by the Bernoulli hydrodynamic equation [34]:

$$v_{ej} = \sqrt{\frac{2P}{\rho}}, \tag{9}$$

where ρ is the density. Using (8) and (9), we obtain the ablation rate due to the expulsion of the melted material out of the crater under the action of the plasma recoil pressure as

$$v_{ej} = \sqrt{\frac{2}{\rho}}\left(\frac{fZ}{2(1+\frac{3}{2\alpha})\tau}F_0\right)^{1/4} e^{-\frac{r^2}{2\omega_0^2}}. \tag{10}$$

Equation (10) shows that the ablation rate due to the melt expulsion also has a Gaussian profile with effective spot size of $2\omega_0$. The theoretical analysis indicates that the $2\omega_0$ is the effective beam spot size related to the nanosecond pulsed laser–plasma interaction zone.

The theoretical analysis presented in the previous paragraphs may allow us to evaluate the silicon laser ablation threshold using the experimental results for the crater diameter growth with an applied laser fluence. Considering $2\omega_0$ as an effective spot size, a simple relationship can be derived between the crater diameter, D, and the ablation threshold fluence, F_{th}, at the given shot number. The measured crater diameters, D, are related to the threshold fluence F_{th} via

$$F_{th} = F_0 \exp\left(-\frac{D^2}{8\omega_0^2}\right), \tag{11}$$

where ω_0 is the applied laser beam spot size. By rearranging (11), the diameter, D, of the modified area and the peak laser fluence F_0 at the sample satisfies the following relation:

$$D^2 = 8\omega_0^2\left[\ln(F_0) - \ln(F_{th})\right]. \tag{12}$$

Using (12), the estimated laser beam spot size and the silicon multiple-shot ablation threshold fluence are obtained by fitting the plot of the square of the crater diameter versus the logarithm of the applied laser fluence.

Figures 3 and 4 present the laser fluence and the shot number dependence of silicon laser ablation in the DMSO and the water interfaces using nanosecond pulsed laser irradiation at 532 nm. The square of an experimentally ablated crater diameter growth with the respect to the logarithm of the applied laser fluence are shown for $N = 5$, 10, 50, 100, 500 laser pulses. Note that the silicon laser ablations in the DMSO confinement have smaller crater diameter size compared to the water. It is clearly indicated in these figures that the square of ablated spots diameter increases linearly with the logarithm of the applied laser fluence. A linear regression fit of the experimental data to (12), provide a slope that gave the laser beam a diameter and an intercept for each line at $D^2 = 0$ to get the silicon ablation threshold. The average estimated laser beam spot size in the DMSO and the water are found to be 145 ± 5 and 163 ± 4 μm, respectively. Excellent agreement is obtained between the estimated laser beam spot size and the experimental measurement value of 150 μm. The silicon's multiple-shot thresholds are summarized in Table 1.

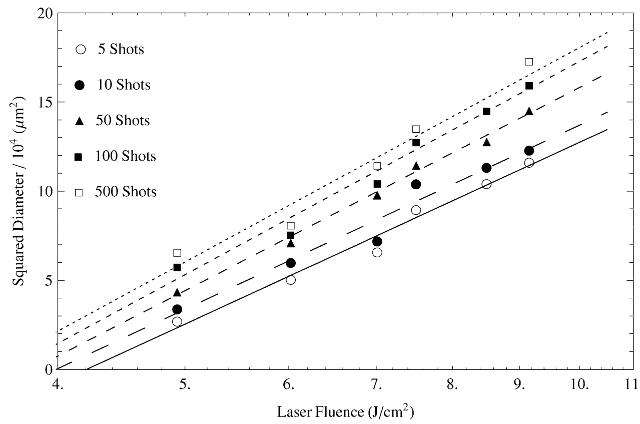

Fig. 3 Dependence of the silicon ablation threshold at different shot number, 5(○), 10(●), 50(▲), 100(■), and 500(□) laser pulses, in the DMSO. The *solid*, *long dash*, *middle dash*, *small dash*, and *dotted lines* show the fits to (12) with $F_{th}(5) = 4.2$ J/cm^2, $\omega_0(5) = 140$ μm, $F_{th}(10) = 4.0$ J/cm^2, $\omega_0(10) = 140$ μm, $F_{th}(50) = 3.8$ J/cm^2, $\omega_0(50) = 145$ μm, $F_{th}(100) = 3.7$ J/cm^2, $\omega_0(100) = 150$ μm, $F_{th}(500) = 3.4$ J/cm^2, $\omega_0(500) = 150$ μm, respectively

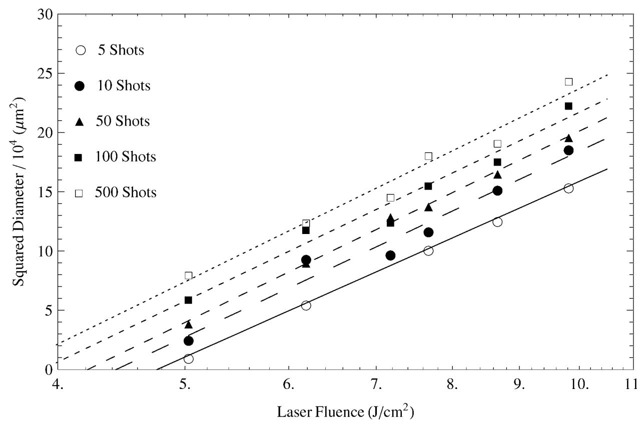

Fig. 4 Dependence of the silicon ablation threshold at different shots number, 5(○), 10(●), 50(▲), 100(■), and 500(□) laser pulses, in the water. The *solid*, *long dash*, *middle dash*, *small dash*, and *dotted lines* show the fits to (12) with $F_{th}(5) = 4.8$ J/cm^2, $\omega_0(5) = 155$ μm, $F_{th}(10) = 4.4$ J/cm^2, $\omega_0(10) = 165$ μm, $F_{th}(50) = 4.1$ J/cm^2, $\omega_0(50) = 165$ μm, $F_{th}(100) = 3.9$ J/cm^2, $\omega_0(100) = 165$ μm, $F_{th}(500) = 3.7$ J/cm^2, $\omega_0(500) = 165$ μm, respectively

The ablation threshold fluence decreases with the number of applied laser pulses per spot. Such an accumulative behavior under femtosecond pulse laser illumination has been observed in other materials such as metals [35, 36], ceramics [37], polymers [38], and silicon [39]. The reported results have been explained in terms of an incubation model [40]. In this model, the threshold fluence $F_{th}(N)$ for N pulses is related to the threshold fluence $F_{th}(1)$ for $N = 1$ by a power law

$$F_{th}(N) = F_{th}(1)N^{S-1}. \qquad (13)$$

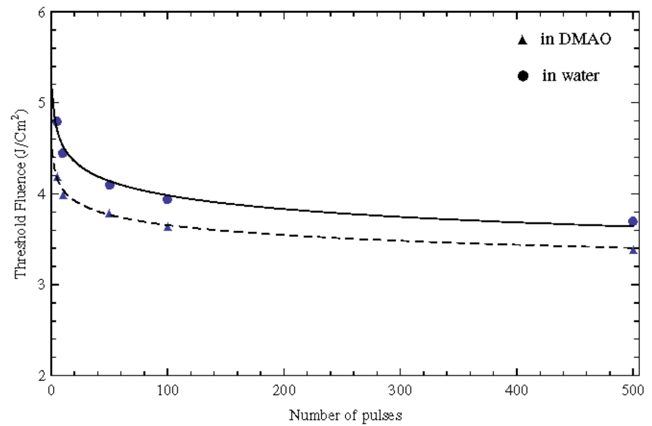

Fig. 5 Shows the experimental results of the ablation threshold versus the number of laser pulses in the DMSO (▲) and the water (●). The *solid* and *dash lines* show the fits to (13) with $F_{th}(1) = 4.4$ J/cm^2 and $S = 0.96$ in the DMSO and $F_{th}(1) = 5.1$ J/cm^2 and $S = 0.94$ in the water, respectively

Table 1 Ablation threshold values, F_{th}, in the DMSO and the water for different number of pulses per spot, N

N	F_{th} (DMSO), J/cm^2	F_{th} (water), J/cm^2
1	4.4	5.1
5	4.2	4.8
10	4.0	4.4
50	3.8	4.1
100	3.7	3.9
500	3.4	3.7

The exponent S characterized the degree of incubation in the materials. For $S = 1$, the threshold fluence is not dependent on the number of pulses, i.e., incubation is absent. Figure 5 confirms the validity of the model for our nanosecond laser ablation of silicon in the DMSO and the water. The fit yields $S = 0.96$ for the DMSO and $S = 0.94$ for the water, respectively. In our results, the least accumulation effect is observed in the DMSO confinement. Using (13), the single-shot ablation threshold for silicon in the DMSO and the water are given in Table 1. Note that the laser ablation of silicon in the DMSO has smaller value for single-shot ablation threshold compared to the value obtained in the water.

4 Conclusions

Pulsed laser ablation of silicon in the dimethyl sulfoxide (DMSO) and the water are investigated at different applied laser fluence levels and laser shot numbers using 15 ns pulsed laser irradiation at 532 nm. The laser-induced surface modifications of silicon are analyzed under repetitive irradiation at different applied laser fluence levels. The analysis of these experimental observations suggests that the formation

of a deep superheated liquid with bubbles and a subsequent melt expulsion could be responsible mechanism for the silicon ablation in the DMSO and the water. Silicon surface ablated diameter growths are measured at different applied laser fluences and shot numbers in the both liquid interfaces. The silicon laser-induced surface ablation in the DMSO interface indicates slightly smaller ablated diameter size at a given applied laser fluence compared to the results found in the water. A theoretical analysis is presented to investigate the silicon surface etching in liquid by intense multiple nanosecond laser pulses. The analysis provides a good qualitative description of the behavior of an ablated growth diameter on a material surface due to the action of the liquid-confined plasma pressure. Our results show that the process of melt expulsion is a dominant mechanism for nanosecond pulsed laser ablation of silicon in the DMSO and the water. Single- and multiple-shot laser ablation thresholds of silicon are determined. Smaller single- and multiple-shot ablation thresholds and similar incubation factors were found under the DMSO confinement in comparison with the results obtained in the water. These results show that the DMSO is also a good candidate for liquid-assisted semiconductor processing.

References

1. J. Ohara, M. Nagakubo, N. Kawahara, T. Hattori, *Proceedings of the IEEE, Tenth Annual International Workshop on Micro Electro Mechanical Systems* (IEEE Press, New York, 1997), pp. 175–179
2. S.I. Dolgaev, A.A. Lyalin, G.A. Shafeev, V.V. Voronov, Appl. Phys. A **63**, 75 (1996)
3. S. Zhu, Y.F. Lu, M.H. Hong, X.Y. Chen, J. Appl. Phys. **89**, 2400 (2001)
4. B.N. Chichkov, C. Momma, S. Nolte, F. Von Alvensleben, A. Tünnermann, Appl. Phys. A **63**, 109 (1996)
5. F. Sanchez, J.L. Morenza, R. Aguiar, J.C. Delgado, M. Varela, Appl. Phys. Lett. **69**, 620 (1996)
6. A.J. Pedraza, J.D. Fowlkes, D.H. Lowndes, Appl. Phys. Lett. **77**, 3018 (2000)
7. P. Ballard, J. Phys. IV **1**, 493 (1991)
8. P. Peyre, R. Fabbro, L. Berthe, C. Dubouchet, J. Laser Appl. **8**, 135 (1996)
9. A. Kruusing, Opt. Lasers Eng. **41**, 329 (2004)
10. J. Ren, M. Kelly, L. Hesselink, Opt. Lett. **30**, 1740 (2005)
11. K.L. Choo, Y. Ogawa, G. Kanbargi, V. Otra, L.M. Raff, R. Komanduri, Mater. Sci. Eng. A **372**, 145 (2004)
12. J.H. Yoo, S.H. Jeong, R. Greif, R.E. Russo, J. Appl. Phys. **88**, 1638 (2000)
13. Ž. Andreić, V. Henč-Bartolič, D. Gracin, M. Stubičar, Appl. Surf. Sci. **136**, 73 (1998)
14. V.V. Voronov, S.I. Dolgaev, A.A. Lyalin, G.A. Shafeev, Quantum Electron. **26**, 621 (1996)
15. S.I. Dolgaev, V.V. Voronov, G.A. Shafeev, C. Fauquet-Ben Ammar, J.-M. Themlin, A. Cros, W. Marine, Appl. Surf. Sci. **109–110**, 559 (1997)
16. G.A. Shafeev, E.D. Obraztsova, S.M. Pimenov, Appl. Phys. A **65**, 29 (1997)
17. G.A. Shafeev, E.D. Obraztsova, S.M. Pimenov, Mater. Sci. Eng. B **46**, 129 (1997)
18. G.A. Shafeev, Proc. SPIE **3484**, 149 (1998)
19. V. Craciun, N. Bassim, R.K. Singh, D. Craciun, J. Hermann, C. Boulmer-Leborgne, Appl. Surf. Sci. **186**, 288 (2002)
20. M. Amer, L. Dosser, S. LeClair, J.F. Maguire, Appl. Surf. Sci. **187**, 291 (2002)
21. V.I. Emel'yanov, D.V. Babak, Appl. Phys. A **74**, 797 (2002)
22. J.M. Liu, Opt. Lett. **7**, 196 (1982)
23. S. Baudach, J. Bonse, W. Kautek, Appl. Phys. A **69**, 395 (1999)
24. C.A. MacDonald, A.M. Malvezzi, F. Spaepen, J. Appl. Phys. **65**, 129 (1999)
25. J. Jandeleit, G. Urbasch, H.D. Hoffmann, H.-G. Treusch, E.W. Kreutz, Appl. Phys. A **63**, 117 (1996)
26. K. Venkatakrishnan, P. Stanley, N.R. Sivakumar, B. Tan, L.E.N. Lim, Appl. Phys. A **77**, 655 (2003)
27. W. Kautek, J. Kruger, Proc. SPIE **2207**, 600 (1994)
28. P.T. Mannion, J. Magee, E. Coyne, G.M. O'Conner, T.J. Glynn, Appl. Surf. Sci. **233**, 275 (2004)
29. R. Fabbro, J. Fournier, P. Ballard, D. Devaux, J. Virmont, J. Appl. Phys. **68**, 775 (1990)
30. R.D. Griffin, B.L. Justus, A.J. Campillo, L.S. Goldberg, J. Appl. Phys. **59**, 1968 (1986)
31. L. Tollier, R. Fabbro, E. Bartnicki, J. Appl. Phys. **83**, 1224 (1998)
32. L. Berthe, R. Fabbro, P. Peyre, L. Tollier, E. Bartnicki, J. Appl. Phys. **82**, 2826 (1997)
33. P. Peyre, L. Berthe, X. Scherpereel, R. Fabbro, E. Bartnicki, J. Appl. Phys. **84**, 5985 (1998)
34. M. Stafe, C. Negutu, I.M. Popescu, Appl. Surf. Sci. **253**, 6353 (2007)
35. S.-S. Wellershoff, J. Güdde, J. Hohlfeld, J.G. Müller, E. Matthias, Proc. SPIE **3343**, 378 (1998)
36. J. Güdde, J. Hohlfeld, J.G. Müller, E. Matthias, Appl. Surf. Sci. **127–129**, 40 (1998)
37. J. Bonse, P. Rudolph, J. Krüger, S. Baudach, W. Kautek, Appl. Surf. Sci. **154–155**, 659 (2000)
38. S. Baudach, J. Bonse, J. Krüger, W. Kautek, Appl. Surf. Sci. **154–155**, 555 (2000)
39. J. Bonse, S. Baudach, J. Krüger, W. Kautek, M. Lenzer, Appl. Phys. A **74**, 19 (2002)
40. Y. Jee, M.F. Becker, R.M. Walser, J. Opt. Soc. Am. B **5**, 648 (1988)